Measurement of the $e^+e^- \to \eta J/\psi$ cross section and search for $e^+e^- \to \pi^0 J/\psi$ at center-of-mass energies between 3.810 and 4.600 GeV

M. Ablikim,[1] M. N. Achasov,[9,a] X. C. Ai,[1] O. Albayrak,[5] M. Albrecht,[4] D. J. Ambrose,[44] A. Amoroso,[48a,48c] F. F. An,[1] Q. An,[45] J. Z. Bai,[1] R. Baldini Ferroli,[20a] Y. Ban,[31] D. W. Bennett,[19] J. V. Bennett,[5] M. Bertani,[20a] D. Bettoni,[21a] J. M. Bian,[43] F. Bianchi,[48a,48c] E. Boger,[23,h] O. Bondarenko,[25] I. Boyko,[23] R. A. Briere,[5] H. Cai,[50] X. Cai,[1] O. Cakir,[40a,b] A. Calcaterra,[20a] G. F. Cao,[1] S. A. Cetin,[40b] J. F. Chang,[1] G. Chelkov,[23,c] G. Chen,[1] H. S. Chen,[1] H. Y. Chen,[2] J. C. Chen,[1] M. L. Chen,[1] S. J. Chen,[29] X. Chen,[1] X. R. Chen,[26] Y. B. Chen,[1] H. P. Cheng,[17] X. K. Chu,[31] G. Cibinetto,[21a] D. Cronin-Hennessy,[43] H. L. Dai,[1] J. P. Dai,[34] A. Dbeyssi,[14] D. Dedovich,[23] Z. Y. Deng,[1] A. Denig,[22] I. Denysenko,[23] M. Destefanis,[48a,48c] F. De Mori,[48a,48c] Y. Ding,[27] C. Dong,[30] J. Dong,[1] L. Y. Dong,[1] M. Y. Dong,[1] S. X. Du,[52] P. F. Duan,[1] J. Z. Fan,[39] J. Fang,[1] S. S. Fang,[1] X. Fang,[45] Y. Fang,[1] L. Fava,[48b,48c] F. Feldbauer,[22] G. Felici,[20a] C. Q. Feng,[45] E. Fioravanti,[21a] M. Fritsch,[14] C. D. Fu,[1] Q. Gao,[1] X. Y. Gao,[2] Y. Gao,[39] Z. Gao,[45] I. Garzia,[21a] C. Geng,[45] K. Goetzen,[10] W. X. Gong,[1] W. Gradl,[22] M. Greco,[48a,48c] M. H. Gu,[1] Y. T. Gu,[12] Y. H. Guan,[1] A. Q. Guo,[1] L. B. Guo,[28] Y. Guo,[1] Y. P. Guo,[22] Z. Haddadi,[25] A. Hafner,[22] S. Han,[50] Y. L. Han,[1] X. Q. Hao,[15] F. A. Harris,[42] K. L. He,[1] Z. Y. He,[30] T. Held,[4] Y. K. Heng,[1] Z. L. Hou,[1] C. Hu,[28] H. M. Hu,[1] J. F. Hu,[48a,48c] T. Hu,[1] Y. Hu,[1] G. M. Huang,[6] G. S. Huang,[45] H. P. Huang,[50] J. S. Huang,[15] X. T. Huang,[33] Y. Huang,[29] T. Hussain,[47] Q. Ji,[1] Q. P. Ji,[30] X. B. Ji,[1] X. L. Ji,[1] L. L. Jiang,[1] L. W. Jiang,[50] X. S. Jiang,[1] J. B. Jiao,[33] Z. Jiao,[17] D. P. Jin,[1] S. Jin,[1] T. Johansson,[49] A. Julin,[43] N. Kalantar-Nayestanaki,[25] X. L. Kang,[1] X. S. Kang,[30] M. Kavatsyuk,[25] B. C. Ke,[5] R. Kliemt,[14] B. Kloss,[22] O. B. Kolcu,[40b,d] B. Kopf,[4] M. Kornicer,[42] W. Kuehn,[24] A. Kupsc,[49] W. Lai,[1] J. S. Lange,[24] M. Lara,[19] P. Larin,[14] C. Leng,[48c] C. H. Li,[1] Cheng Li,[45] D. M. Li,[52] F. Li,[1] G. Li,[1] H. B. Li,[1] J. C. Li,[1] Jin Li,[32] K. Li,[13] K. Li,[33] Lei Li,[3] P. R. Li,[41] T. Li,[33] W. D. Li,[1] W. G. Li,[1] X. L. Li,[33] X. M. Li,[12] X. N. Li,[1] X. Q. Li,[30] Z. B. Li,[38] H. Liang,[45] Y. F. Liang,[36] Y. T. Liang,[24] G. R. Liao,[11] D. X. Lin,[14] B. J. Liu,[1] C. X. Liu,[1] F. H. Liu,[35] Fang Liu,[1] Feng Liu,[6] H. B. Liu,[12] H. H. Liu,[16] H. H. Liu,[1] H. M. Liu,[1] J. Liu,[1] J. P. Liu,[50] J. Y. Liu,[1] K. Liu,[39] K. Y. Liu,[27] L. D. Liu,[31] P. L. Liu,[1] Q. Liu,[41] S. B. Liu,[45] X. Liu,[26] X. X. Liu,[41] Y. B. Liu,[30] Z. A. Liu,[1] Zhiqiang Liu,[1] Zhiqing Liu,[22] H. Loehner,[25] X. C. Lou,[1,e] H. J. Lu,[17] J. G. Lu,[1] R. Q. Lu,[18] Y. Lu,[1] Y. P. Lu,[1] C. L. Luo,[28] M. X. Luo,[51] T. Luo,[42] X. L. Luo,[1] M. Lv,[1] X. R. Lyu,[41] F. C. Ma,[27] H. L. Ma,[1] L. L. Ma,[33] Q. M. Ma,[1] S. Ma,[1] T. Ma,[1] X. N. Ma,[30] X. Y. Ma,[1] F. E. Maas,[14] M. Maggiora,[48a,48c] Q. A. Malik,[47] Y. J. Mao,[31] Z. P. Mao,[1] S. Marcello,[48a,48c] J. G. Messchendorp,[25] J. Min,[1] T. J. Min,[1] R. E. Mitchell,[19] X. H. Mo,[1] Y. J. Mo,[6] C. Morales Morales,[14] K. Moriya,[19] N. Yu. Muchnoi,[9,a] H. Muramatsu,[43] Y. Nefedov,[23] F. Nerling,[14] I. B. Nikolaev,[9,a] Z. Ning,[1] S. Nisar,[8] S. L. Niu,[1] X. Y. Niu,[1] S. L. Olsen,[32] Q. Ouyang,[1] S. Pacetti,[20b] P. Patteri,[20a] M. Pelizaeus,[4] H. P. Peng,[45] K. Peters,[10] J. Pettersson,[49] J. L. Ping,[28] R. G. Ping,[1] R. Poling,[43] Y. N. Pu,[18] M. Qi,[29] S. Qian,[1] C. F. Qiao,[41] L. Q. Qin,[33] N. Qin,[50] X. S. Qin,[1] Y. Qin,[31] Z. H. Qin,[1] J. F. Qiu,[1] K. H. Rashid,[47] C. F. Redmer,[22] H. L. Ren,[18] M. Ripka,[22] G. Rong,[1] Ch. Rosner,[14] X. D. Ruan,[12] V. Santoro,[21a] A. Sarantsev,[23,f] M. Savrié,[21b] K. Schoenning,[49] S. Schumann,[22] W. Shan,[31] M. Shao,[45] C. P. Shen,[2] P. X. Shen,[30] X. Y. Shen,[1] H. Y. Sheng,[1] W. M. Song,[1] X. Y. Song,[1] S. Sosio,[48a,48c] S. Spataro,[48a,48c] G. X. Sun,[1] J. F. Sun,[15] S. S. Sun,[1] Y. J. Sun,[45] Y. Z. Sun,[1] Z. J. Sun,[1] Z. T. Sun,[19] C. J. Tang,[36] X. Tang,[1] I. Tapan,[40c] E. H. Thorndike,[44] M. Tiemens,[25] D. Toth,[43] M. Ullrich,[24] I. Uman,[40b] G. S. Varner,[42] B. Wang,[30] B. L. Wang,[41] D. Wang,[31] D. Y. Wang,[31] K. Wang,[1] L. L. Wang,[1] L. S. Wang,[1] M. Wang,[33] P. Wang,[1] P. L. Wang,[1] Q. J. Wang,[1] S. G. Wang,[31] W. Wang,[1] X. F. Wang,[39] Y. D. Wang,[14] Y. D. Wang,[20a] Y. F. Wang,[1] Y. Q. Wang,[22] Z. Wang,[1] Z. G. Wang,[1] Z. H. Wang,[45] Z. Y. Wang,[1] T. Weber,[22] D. H. Wei,[11] J. B. Wei,[31] P. Weidenkaff,[22] S. P. Wen,[1] U. Wiedner,[4] M. Wolke,[49] L. H. Wu,[1] Z. Wu,[1] L. G. Xia,[39] Y. Xia,[18] D. Xiao,[1] Z. J. Xiao,[28] Y. G. Xie,[1] Q. L. Xiu,[1] G. F. Xu,[1] L. Xu,[1] Q. J. Xu,[13] Q. N. Xu,[41] X. P. Xu,[37] L. Yan,[45] W. B. Yan,[45] W. C. Yan,[45] Y. H. Yan,[18] H. X. Yang,[1] L. Yang,[50] Y. Yang,[6] Y. X. Yang,[11] H. Ye,[1] M. Ye,[1] M. H. Ye,[7] J. H. Yin,[1] B. X. Yu,[1] C. X. Yu,[30] H. W. Yu,[31] J. S. Yu,[26] C. Z. Yuan,[1] W. L. Yuan,[29] Y. Yuan,[1] A. Yuncu,[40b,g] A. A. Zafar,[47] A. Zallo,[20a] Y. Zeng,[18] B. X. Zhang,[1] B. Y. Zhang,[1] C. Zhang,[29] C. C. Zhang,[1] D. H. Zhang,[1] H. H. Zhang,[38] H. Y. Zhang,[1] J. J. Zhang,[1] J. L. Zhang,[1] J. Q. Zhang,[1] J. W. Zhang,[1] J. Y. Zhang,[1] J. Z. Zhang,[1] K. Zhang,[1] L. Zhang,[1] S. H. Zhang,[1] X. Y. Zhang,[33] Y. Zhang,[1] Y. H. Zhang,[1] Y. T. Zhang,[45] Z. H. Zhang,[6] Z. P. Zhang,[45] Z. Y. Zhang,[50] G. Zhao,[1] J. W. Zhao,[1] J. Y. Zhao,[1] J. Z. Zhao,[1] Lei Zhao,[45] Ling Zhao,[1] M. G. Zhao,[30] Q. Zhao,[1] Q. W. Zhao,[1] S. J. Zhao,[52] T. C. Zhao,[1] Y. B. Zhao,[1] Z. G. Zhao,[45] A. Zhemchugov,[23,h] B. Zheng,[46] J. P. Zheng,[1] W. J. Zheng,[33] Y. H. Zheng,[41] B. Zhong,[28] L. Zhou,[1] Li Zhou,[30] X. Zhou,[50] X. K. Zhou,[45] X. R. Zhou,[45] X. Y. Zhou,[1] K. Zhu,[1] K. J. Zhu,[1] S. Zhu,[1] X. L. Zhu,[39] Y. C. Zhu,[45] Y. S. Zhu,[1] Z. A. Zhu,[1] J. Zhuang,[1] L. Zotti,[48a,48c] B. S. Zou,[1] and J. H. Zou[1]

(BESIII Collaboration)

[1]*Institute of High Energy Physics, Beijing 100049, People's Republic of China*
[2]*Beihang University, Beijing 100191, People's Republic of China*
[3]*Beijing Institute of Petrochemical Technology, Beijing 102617, People's Republic of China*
[4]*Bochum Ruhr-University, D-44780 Bochum, Germany*
[5]*Carnegie Mellon University, Pittsburgh, Pennsylvania 15213, USA*
[6]*Central China Normal University, Wuhan 430079, People's Republic of China*
[7]*China Center of Advanced Science and Technology, Beijing 100190, People's Republic of China*
[8]*COMSATS Institute of Information Technology, Lahore, Defence Road, Off Raiwind Road, 54000 Lahore, Pakistan*
[9]*G.I. Budker Institute of Nuclear Physics SB RAS (BINP), Novosibirsk 630090, Russia*
[10]*GSI Helmholtzcentre for Heavy Ion Research GmbH, D-64291 Darmstadt, Germany*
[11]*Guangxi Normal University, Guilin 541004, People's Republic of China*
[12]*GuangXi University, Nanning 530004, People's Republic of China*
[13]*Hangzhou Normal University, Hangzhou 310036, People's Republic of China*
[14]*Helmholtz Institute Mainz, Johann-Joachim-Becher-Weg 45, D-55099 Mainz, Germany*
[15]*Henan Normal University, Xinxiang 453007, People's Republic of China*
[16]*Henan University of Science and Technology, Luoyang 471003, People's Republic of China*
[17]*Huangshan College, Huangshan 245000, People's Republic of China*
[18]*Hunan University, Changsha 410082, People's Republic of China*
[19]*Indiana University, Bloomington, Indiana 47405, USA*
[20a]*INFN Laboratori Nazionali di Frascati, I-00044 Frascati, Italy*
[20b]*INFN and University of Perugia, I-06100 Perugia, Italy*
[21a]*INFN Sezione di Ferrara, I-44122 Ferrara, Italy*
[21b]*University of Ferrara, I-44122 Ferrara, Italy*
[22]*Johannes Gutenberg University of Mainz, Johann-Joachim-Becher-Weg 45, D-55099 Mainz, Germany*
[23]*Joint Institute for Nuclear Research, 141980 Dubna, Moscow Region, Russia*
[24]*Justus Liebig University Giessen, II. Physikalisches Institut, Heinrich-Buff-Ring 16, D-35392 Giessen, Germany*
[25]*KVI-CART, University of Groningen, NL-9747 AA Groningen, The Netherlands*
[26]*Lanzhou University, Lanzhou 730000, People's Republic of China*
[27]*Liaoning University, Shenyang 110036, People's Republic of China*
[28]*Nanjing Normal University, Nanjing 210023, People's Republic of China*
[29]*Nanjing University, Nanjing 210093, People's Republic of China*
[30]*Nankai University, Tianjin 300071, People's Republic of China*
[31]*Peking University, Beijing 100871, People's Republic of China*
[32]*Seoul National University, Seoul 151-747, Korea*
[33]*Shandong University, Jinan 250100, People's Republic of China*
[34]*Shanghai Jiao Tong University, Shanghai 200240, People's Republic of China*
[35]*Shanxi University, Taiyuan 030006, People's Republic of China*
[36]*Sichuan University, Chengdu 610064, People's Republic of China*
[37]*Soochow University, Suzhou 215006, People's Republic of China*
[38]*Sun Yat-Sen University, Guangzhou 510275, People's Republic of China*
[39]*Tsinghua University, Beijing 100084, People's Republic of China*
[40a]*Istanbul Aydin University, 34295 Sefakoy, Istanbul, Turkey*
[40b]*Dogus University, 34722 Istanbul, Turkey*
[40c]*Uludag University, 16059 Bursa, Turkey*
[41]*University of Chinese Academy of Sciences, Beijing 100049, People's Republic of China*
[42]*University of Hawaii, Honolulu, Hawaii 96822, USA*
[43]*University of Minnesota, Minneapolis, Minnesota 55455, USA*
[44]*University of Rochester, Rochester, New York 14627, USA*
[45]*University of Science and Technology of China, Hefei 230026, People's Republic of China*
[46]*University of South China, Hengyang 421001, People's Republic of China*
[47]*University of the Punjab, Lahore 54590, Pakistan*
[48a]*University of Turin, I-10125 Turin, Italy*
[48b]*University of Eastern Piedmont, I-15121 Alessandria, Italy*
[48c]*INFN, I-10125 Turin, Italy*
[49]*Uppsala University, Box 516, SE-75120 Uppsala, Sweden*

[50]Wuhan University, Wuhan 430072, People's Republic of China
[51]Zhejiang University, Hangzhou 310027, People's Republic of China
[52]Zhengzhou University, Zhengzhou 450001, People's Republic of China
(Received 23 March 2015; published 9 June 2015)

Using data samples collected with the BESIII detector operating at the BEPCII collider at 17 center-of-mass energies from 3.810 to 4.600 GeV, we perform a study of $e^+e^- \to \eta J/\psi$ and $\pi^0 J/\psi$. The Born cross sections of these two processes are measured at each center-of-mass energy. The measured energy-dependent Born cross section for $e^+e^- \to \eta J/\psi$ shows an enhancement around 4.2 GeV. The measurement is compatible with an earlier measurement by Belle.

DOI: 10.1103/PhysRevD.91.112005 PACS numbers: 13.25.Gv, 13.66.Bc, 14.40.Pq, 14.40.Rt

I. INTRODUCTION

During the last decade, new charmoniumlike vector states, such as the $Y(4260)$, $Y(4360)$ and $Y(4660)$, have been observed by *BABAR* [1,2], Belle [3–6] and CLEO [7]. The masses of these new Y states are above the $D\bar{D}$ production threshold, ranging from 4.0 to 4.7 GeV/c^2. Since all of them are produced in e^+e^- annihilation [either directly or via the initial state radiation (ISR) process], and since they have been observed to decay in dipion hadronic transitions to the J/ψ or $\psi(3686)$, one would naturally interpret these states as vector charmonium excitations. However, peculiar features of these Y states reveal an exotic nature that likely excludes a conventional charmonium interpretation. These features include a discrepancy with the spectrum of vector charmonium states predicted by the potential model given in Ref. [8], a surprisingly large coupling to final states without open-charm mesons [9,10] and a lack of observation in the inclusive hadronic cross section [11]. Also, very recently, several charged charmoniumlike states—the $Z_c(3900)^{\pm}$ [4,12,13], $Z_c(3885)^{\pm}$ [14], $Z_c(4020)^{\pm}$ [15], $Z_c(4025)^{\pm}$ [16], as well as their isospin partners, the neutral states $Z_c(3900)^0$ [13] and $Z_c(4020)^0$ [17]—were observed in the same mass region as these Y states. This suggests that the nature of the Y states could be related to that of the Z_c states. Moreover, the observed cross sections as a function of center-of-mass (c.m.) energy for $e^+e^- \to \pi^+\pi^- J/\psi$ [1,3,4,7], $\pi^+\pi^-\psi(3686)$ [2,5,6], $\pi^+\pi^- h_c$ [15], $\eta J/\psi$ [18] and $\omega\chi_{c0}$ [19] are inconsistent with each other. These observations hint at the existence of a more complicated and mysterious underlying dynamics.

Many theoretical interpretations have been proposed to classify these Y states, such as hybrid charmonium [20], tetraquark [21] or hadronic molecule [22] models, but none of them has been able to describe all experimental observations in all aspects. Searching for new decay modes and measuring the line shapes of their production cross sections will be very helpful for these Y states interpretations. Hadronic transitions (by η, π^0 or a pion pair) to lower charmonia like the J/ψ are also regarded as sensitive probes to study the properties of these Y states [23].

The cross sections of $e^+e^- \to \eta J/\psi$ and $\pi^0 J/\psi$ above the $D\bar{D}$ production threshold have been evaluated within a nonrelativistic framework derived from QCD [24], and their line shapes are predicted to be strongly affected by open charm effects [25]. Belle, BESIII and CLEO-c have measured the production cross sections of $e^+e^- \to \eta J/\psi$ above the open-charm threshold [18,26,27]. However, Belle and CLEO-c results suffer from large statistical uncertainties. BESIII reported on a more accurate result, but the measurement was limited to a single c.m. energy of $\sqrt{s} = 4.009$ GeV. Experimental studies with large data samples in a broad energy region may shed light on the nature of the Y states.

In this paper, we report a measurement of the Born cross sections of $e^+e^- \to \eta J/\psi$ and $\pi^0 J/\psi$ at 17 c.m. energies from 3.810 to 4.600 GeV. The data samples are taken by the BESIII detector at the BEPCII collider [28] and are listed in Tables I and II. The c.m. energies are measured with a beam-energy measurement system [29] with an uncertainty of ± 1.0 MeV. In our analysis, the η and π^0 are reconstructed in their two-photon decay mode and the J/ψ via its decay into lepton pairs ($\ell^+\ell^-$).

II. DETECTOR AND MONTE CARLO SIMULATION

BEPCII [28] is a double-ring e^+e^- collider running at c.m. energies ranging from 2.0 to 4.6 GeV, and providing a

[a]Also at the Novosibirsk State University, Novosibirsk, 630090, Russia.
[b]Also at Ankara University, 06100 Tandogan, Ankara, Turkey.
[c]Also at the Moscow Institute of Physics and Technology, Moscow 141700, Russia and at the Functional Electronics Laboratory, Tomsk State University, Tomsk 634050, Russia.
[d]Present address: Istanbul Arel University, 34295 Istanbul, Turkey.
[e]Also at University of Texas at Dallas, Richardson, Texas 75083, USA.
[f]Also at the NRC "Kurchatov Institute," PNPI, 188300 Gatchina, Russia.
[g]Also at Bogazici University, 34342 Istanbul, Turkey.
[h]Also at the Moscow Institute of Physics and Technology, Moscow 141700, Russia.

TABLE I. Results on $e^+e^- \to \eta J/\psi$ in data samples in which a signal is observed with a statistical significance larger than 5σ. The table shows the c.m. energy $\sqrt{s}$, integrated luminosity $\mathcal{L}_{\rm int}$, number of observed η events $N_\eta^{\rm obs}(\mu^+\mu^-)/N_\eta^{\rm obs}(e^+e^-)$ from the fit, efficiency ϵ_μ/ϵ_e, radiative correction factor $(1+\delta^r)$, vacuum polarization factor $(1+\delta^v)$, Born cross section $\sigma^B(\mu^+\mu^-)/\sigma^B(e^+e^-)$, combined Born cross section $\sigma^B_{\rm Com}$ and statistical significance. The first uncertainties are statistical and the second systematic.

$\sqrt{s}$ (GeV)	$\mathcal{L}$(pb^{-1})	$N_\eta^{\rm obs}(\mu^+\mu^-)$	$N_\eta^{\rm obs}(e^+e^-)$	ϵ_μ(%)	ϵ_e(%)	$(1+\delta^r)$	$(1+\delta^v)$	$\sigma^B(\mu^+\mu^-)$ (pb)	$\sigma^B(e^+e^-)$ (pb)	$\sigma^B_{\rm Com}$ (pb)	Significance
4.190	43.1	17.5 ± 4.3	10.4 ± 3.6	35.2	24.1	0.866	1.056	$53.7 \pm 13.2 \pm 3.1$	$46.6 \pm 16.1 \pm 1.7$	$50.8 \pm 10.2 \pm 2.1$	8.4σ
4.210	54.6	25.7 ± 5.1	14.8 ± 4.5	33.7	23.1	0.914	1.057	$61.6 \pm 12.2 \pm 4.1$	$51.7 \pm 15.7 \pm 4.5$	$57.8 \pm 9.6 \pm 3.2$	10.8σ
4.220	54.1	32.6 ± 5.8	11.4 ± 3.9	33.1	22.8	0.937	1.057	$78.2 \pm 13.9 \pm 5.0$	$39.6 \pm 13.6 \pm 2.9$	$57.7 \pm 9.7 \pm 3.0$	12.0σ
4.230	1091.7	394.3 ± 20.9	274.9 ± 20.1	32.4	22.3	0.960	1.056	$46.8 \pm 2.5 \pm 2.5$	$47.3 \pm 3.5 \pm 3.4$	$47.0 \pm 2.0 \pm 2.2$	$>37.0\sigma$
4.245	55.6	9.3 ± 3.3	9.7 ± 3.6	31.4	21.7	0.992	1.056	$21.6 \pm 7.7 \pm 2.4$	$32.6 \pm 12.1 \pm 3.5$	$24.8 \pm 6.5 \pm 2.0$	5.1σ
4.260	825.7	94.4 ± 10.5	75.9 ± 11.9	30.3	20.9	1.021	1.054	$14.9 \pm 1.7 \pm 1.1$	$17.4 \pm 2.7 \pm 1.2$	$15.7 \pm 1.4 \pm 0.9$	17.3σ
4.360	539.8	19.8 ± 5.3	23.9 ± 7.7	25.7	17.7	1.168	1.051	$4.9 \pm 1.3 \pm 0.7$	$8.7 \pm 2.8 \pm 1.1$	$5.6 \pm 1.2 \pm 0.6$	6.2σ
4.420	1074.7	56.9 ± 8.2	42.6 ± 9.9	24.2	16.7	1.225	1.053	$7.3 \pm 1.1 \pm 0.8$	$7.8 \pm 1.8 \pm 0.7$	$7.5 \pm 0.9 \pm 0.6$	11.5σ

peak luminosity of 0.85×10^{33} cm^{-2} s^{-1} at the c.m. energy of 3.770 GeV. The BESIII [28] detector has a geometrical acceptance of 93% of 4π and has four main components. (1) A small-cell, helium-based (40% He, 60% C_3H_8) main drift chamber (MDC) with 43 layers provides an average single-hit resolution of 135 μm, and a charged-particle momentum resolution in a 1 T magnetic field of 0.5% at 1.0 GeV/c. (2) A time-of-flight system is constructed of 5 cm thick plastic scintillators, with 176 detectors of 2.4 m length in two layers in the barrel and 96 fan-shaped detectors in the end caps. The barrel (end cap) time resolution of 80 ps (110 ps) provides a 2σ K/π separation for momenta up to $\sim$1 GeV/c. (3) An electromagnetic calorimeter (EMC) consists of 6240 CsI(Tl) crystals in a cylindrical structure (barrel) and two end caps. The photon energy resolution at 1.0 GeV/c is 2.5% (5%) in the barrel (end caps), and the position resolution is 6 mm (9 mm) in the barrel (end caps). (4) The muon system (MUC) is located in the iron flux return yoke of the superconducting solenoid and consists of 1000 m^2 of Resistive Plate Chambers in nine barrel and eight end cap layers. It provides a position resolution of 2.0 cm.

The optimization of the selection criteria, the determination of detection efficiencies and the estimations of potential backgrounds are performed based on Monte Carlo (MC) simulations taking various aspects of the experimental setup into account. GEANT4-based [30] MC simulation software, which includes the geometric and material description of the BESIII detector, the detector response and digitization models, as well as accounting of the detector running conditions and performances, is used to generate MC samples. In the simulation, the electron-positron collision is simulated with the KKMC [31,32] generator taking into consideration the spread in the beam energy and ISR. In this analysis, large signal MC samples of $e^+e^- \to \eta J/\psi$ and $e^+e^- \to \pi^0 J/\psi$ are generated at c.m. energies corresponding to the experimental values, where the line shape of the production cross section of these two processes, assumed to be identical, is taken from the Belle experiment [18].

III. EVENT SELECTION

The candidate events of $e^+e^- \to \eta J/\psi$ and $\pi^0 J/\psi$ are required to have two charged tracks with a total net charge of zero and at least two photon candidates.

Charged tracks are reconstructed from the hits in the MDC. Each charged track is required to have a polar angle that is well within the fiducial volume of the MDC,

TABLE II. Upper limits of $e^+e^- \to \eta J/\psi$ using the $\mu^+\mu^-$ mode. The table shows the c.m. energy $\sqrt{s}$, integrated luminosity $\mathcal{L}_{\rm int}$, number of observed η events $N_\eta^{\rm sg}$, number of backgrounds from the η sideband $N_\eta^{\rm sb}$ and from the J/ψ sideband $N_{J/\psi}^{\rm sb}$, efficiency ϵ, upper limit of signal number with the consideration of selection efficiency $N_\eta^{\rm up}/\epsilon$ (at the 90% C.L.), radiative correction factor $(1+\delta^r)$, vacuum polarization factor $(1+\delta^v)$, Born cross section σ^B and upper limit on the Born cross sections $\sigma^B_{\rm up}$ (at the 90% C.L.). The first uncertainties are statistical and the second systematic.

$\sqrt{s}$ (GeV)	$\mathcal{L}$(pb^{-1})	$N_\eta^{\rm sg}$	$N_\eta^{\rm sb}$	$N_{J/\psi}^{\rm sb}$	ϵ(%)	$N_\eta^{\rm up}/\epsilon$	$(1+\delta^r)$	$(1+\delta^v)$	σ^B (pb)	$\sigma^B_{\rm up}$ (pb)
3.810	50.5	5	9	11	32.3	<23.3	1.243	1.056	$5.5^{+7.1}_{-4.6} \pm 0.2$	<15.1
3.900	52.6	5	8	7	38.3	<20.9	0.775	1.049	$7.9^{+9.2}_{-5.9} \pm 0.3$	<20.8
4.090	52.6	7	7	5	31.0	<36.3	1.087	1.052	$12.2^{+9.0}_{-6.2} \pm 0.9$	<25.9
4.310	44.9	1	4	2	27.4	<11.7	1.105	1.053	$0.0^{+7.2}_{-2.9} \pm 0.0$	<9.5
4.390	55.2	5	1	4	25.0	<38.4	1.198	1.051	$11.7^{+8.5}_{-5.4} \pm 0.6$	<23.5
4.470	109.9	2	12	8	23.5	<14.7	1.258	1.055	$-1.2^{+3.5}_{-1.9} \pm 0.1$	<4.3
4.530	110.0	5	6	4	22.8	<38.2	1.295	1.055	$4.3^{+4.3}_{-2.8} \pm 0.2$	<10.8
4.575	47.7	2	2	1	22.6	<22.5	1.314	1.055	$4.3^{+7.7}_{-3.8} \pm 0.2$	<14.5
4.600	570.0	5	34	19	22.4	<23.0	1.323	1.055	$-0.8^{+0.9}_{-0.6} \pm 0.1$	<1.2

$|\cos\theta| < 0.93$, where θ is the polar angle of the track in the laboratory frame, to have a point of closest approach to the interaction point that is within ± 10 cm along the beam direction and within 1 cm in the radial direction, and to have a momentum p larger than 1.0 GeV/c. Electron and muon separation is carried out by making use of the deposited energy in the EMC. Tracks with an energy deposition of $E < 0.4$ GeV are identified as muons, while tracks with $E/p > 0.8c$ are identified as electrons or positrons.

Photon candidates are reconstructed by isolated showers in the EMC. The photon energy is required to be at least 25 MeV in the barrel ($|\cos\theta| < 0.80$) and 50 MeV in the end caps ($0.86 < |\cos\theta| < 0.92$). To eliminate showers produced by charged particles, the angle between the shower and the nearest charged track must be larger than 20 degrees. A general requirement on the EMC timing ($0 \le T \le 700$ ns) is implemented to suppress detector electronic noise and energy depositions unrelated to the physical event.

A kinematic fit that imposes momentum and energy conservation ($4C$) is implemented under the hypothesis of $e^+e^- \to \gamma\gamma\ell^+\ell^-$ to improve the momentum and energy resolutions of the final-state particles and to reduce the potential backgrounds. The chi-square of the kinematic fit, χ^2_{4C}, is required to be less than 40. If there are more than two photons in an event, the combination of $\gamma\gamma\ell^+\ell^-$ with the least χ^2_{4C} is chosen. To suppress the backgrounds from

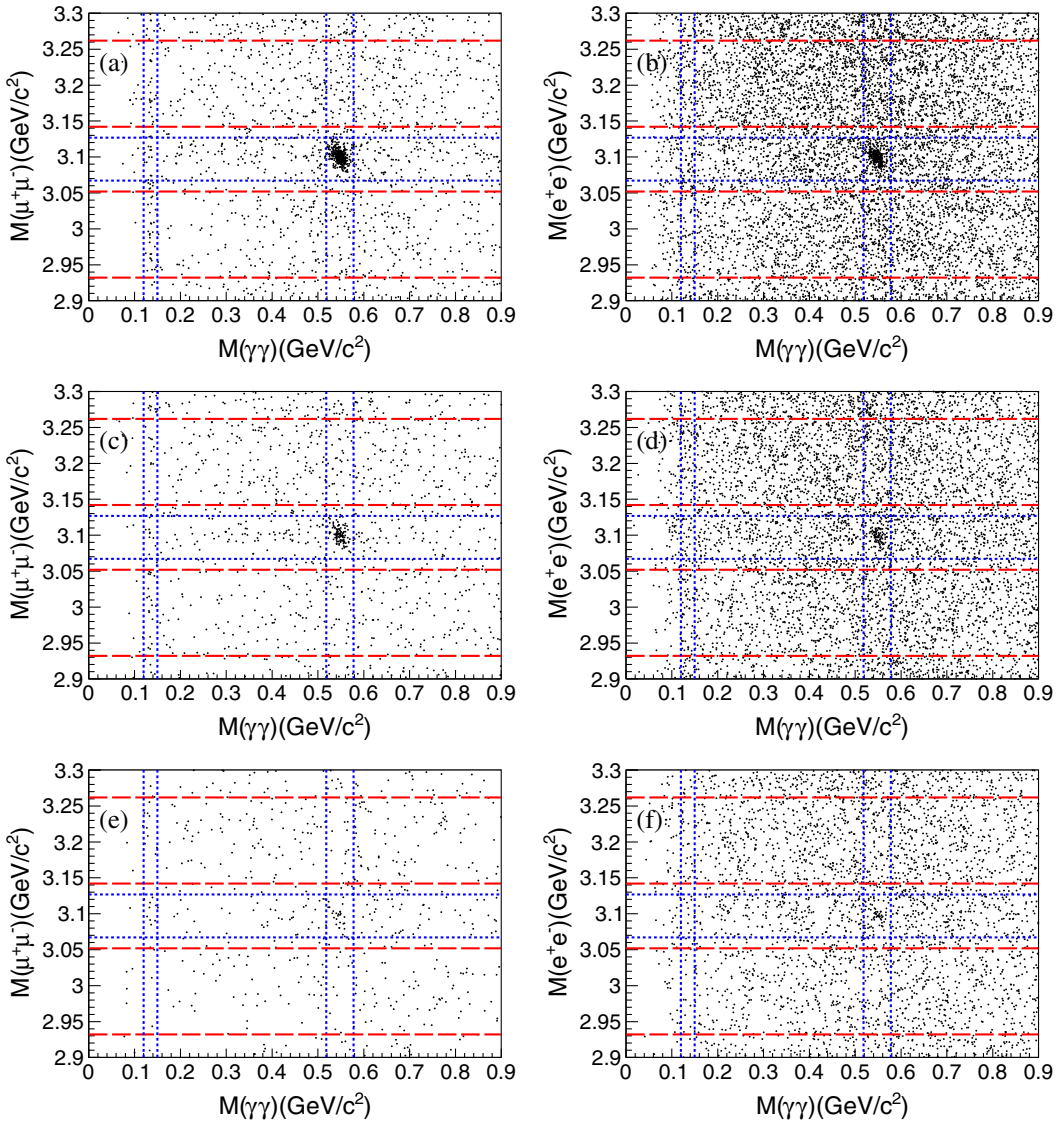

FIG. 1 (color online). Scatter plots of $M(\ell^+\ell^-)$ versus $M(\gamma\gamma)$ for data at $\sqrt{s} = 4.230$ [top panels (a),(b)], 4.260 GeV [middle panels (c),(d)] and 4.360 GeV [bottom panels (c),(d)]. The two panels on the left-hand side correspond to the $\mu^+\mu^-$ mode and the right-hand side to the e^+e^- mode. The blue dotted lines denote the η/π^0 and J/ψ mass bands. The red dashed lines denote the sideband regions of J/ψ.

radiative Bhabha and radiative dimuon events associated with a random photon candidate, the energy of each selected photon is further required to be larger than 80 MeV.

Figure 1 depicts scatter plots of the invariant mass of lepton pairs, $M(\ell^+\ell^-)$, versus that of two photons, $M(\gamma\gamma)$, for data taken at $\sqrt{s} = 4.230$ and 4.260 GeV. A clear accumulation of events is observed around the intersection of the η and J/ψ mass regions, which indicates $e^+e^- \to \eta J/\psi$ signals. There is no significant signal observed around the intersection of the π^0 and J/ψ mass regions. MC studies show that dominant backgrounds are from the radiative Bhabha and dimuon events, and are expected to be distributed uniformly around the J/ψ and η/π^0 mass regions. A significantly larger background yield is observed in the e^+e^- mode than in the $\mu^+\mu^-$ mode, which is due to the much larger Bhabha scattering cross section compared with the dimuon cross section. MC simulations show that the resolution of the invariant mass distributions of lepton pairs is about 10.7 MeV/c^2 for the $\mu^+\mu^-$ mode and 11.5 MeV/c^2 for the e^+e^- mode. The candidate event of $e^+e^- \to \eta J/\psi$ is required to be within the J/ψ signal region, defined as $3.067 < M(\ell^+\ell^-) < 3.127$ GeV/c^2. Sideband regions, defined as $2.932 < M(\ell^+\ell^-) < 3.052$ GeV/c^2 and $3.142 < M(\ell^+\ell^-) < 3.262$ GeV/c^2, four times as wide as the signal region, are used to estimate the non-J/ψ background contributions.

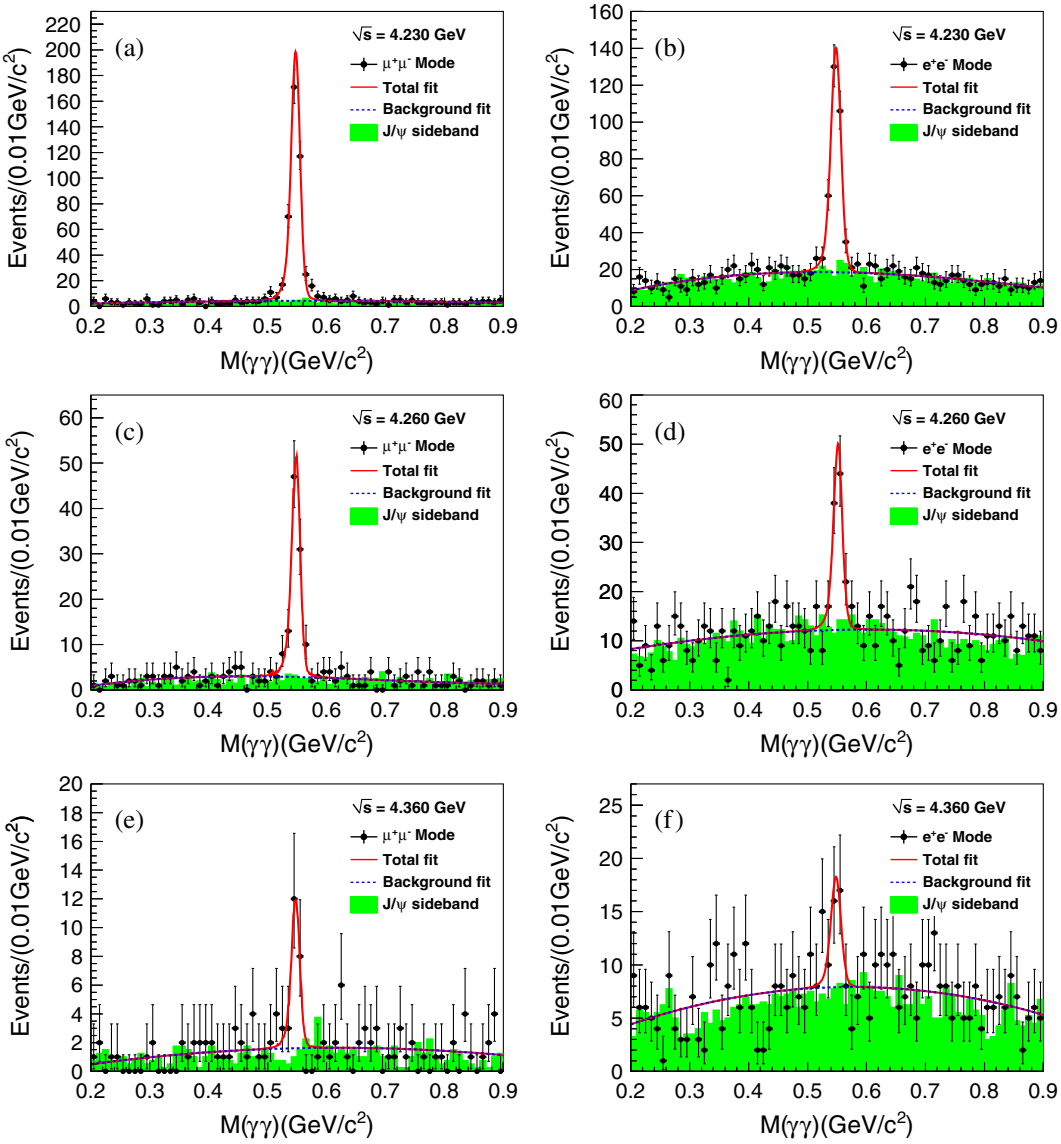

FIG. 2 (color online). Invariant mass distributions of two photons for data at $\sqrt{s} = 4.230$ [top panels (a),(b)], 4.260 GeV [middle panels (c),(d)] and 4.360 GeV [bottom panels (e),(f)]. The left two plots are for the $J/\psi \to \mu^+\mu^-$ mode and the right two for the $J/\psi \to e^+e^-$ mode. Dots with error bars are for data in the J/ψ signal region, the green shaded histograms for the normalized J/ψ sideband events, the red solid curves for the total fit results and the blue dotted curves for the background from the fit.

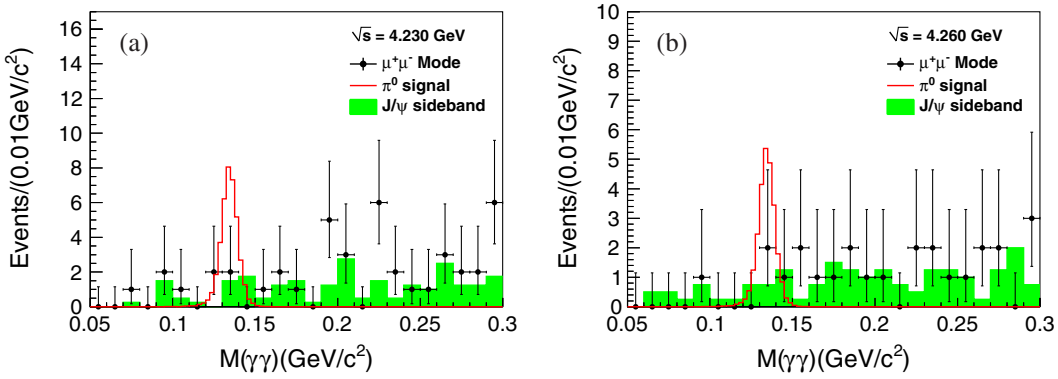

FIG. 3 (color online). Invariant mass distributions of two photons for data at $\sqrt{s} = 4.230$ (a) and 4.260 GeV (b) in the $J/\psi \to \mu^+\mu^-$ mode. Dots with error bars are for data in the J/ψ signal region, the green shaded histograms are the normalized J/ψ sideband events and the red histograms are the π^0 MC signal with arbitrary normalization.

After selecting the J/ψ signal, the invariant mass distributions of two photons, $M(\gamma\gamma)$, are shown in Fig. 2 for data at $\sqrt{s} = 4.230$ and 4.260 GeV. Clear η signals are observed. The corresponding normalized distributions from the events in the J/ψ sideband regions are shown as shaded histograms in the plots. The backgrounds are well described by J/ψ sideband events and show no peaking structure within the η signal region.

The process $e^+e^- \to \pi^0 J/\psi$ is also searched for in the $J/\psi \to \mu^+\mu^-$ mode by analyzing the $M(\gamma\gamma)$ distribution around the π^0 mass region. Such a search is not performed for the $J/\psi \to e^+e^-$ mode due to the large background of radiative Bhabha events. Due to the misidentification of $\pi^\pm$ as $\mu^\pm$, the peaking background from $e^+e^- \to \pi^+\pi^-\pi^0$ would contaminate the π^0 signal for both candidate events within the J/ψ signal or sideband regions. To remove such backgrounds, we require that at least one charged track has a muon counter hit depth larger than 30 cm. Figure 3 shows the $M(\gamma\gamma)$ distributions around the π^0 mass region after this requirement. No significant signal is observed for $\pi^0 \to \gamma\gamma$ decays.

IV. FITS TO THE $M(\gamma\gamma)$ SPECTRUM AND CROSS SECTION RESULTS

After imposing the J/ψ signal selection, an unbinned maximum likelihood fit is performed on $M(\gamma\gamma)$ in the $J/\psi \to e^+e^-$ and $\mu^+\mu^-$ modes, respectively. The probability density function of the $M(\gamma\gamma)$ distribution for η signals is obtained from signal MC simulations convoluted with a Gaussian function, where the Gaussian function describes the difference in resolution between data and MC simulation, and its parameters are left free in the fit. The background shape is described by a second-order Chebyshev polynomial function. The corresponding fit results for $\sqrt{s} = 4.230$ and 4.260 GeV are shown in Fig. 2 and the numbers of η signal events are summarized in Table I. The statistical significances of η signals are larger than 8σ, which are examined using the differences in log-likelihood values of fits with or without an η signal component.

The same event selection criteria and fit procedure on $M(\gamma\gamma)$ are implemented on the other 15 data samples taken at different c.m. energies. We observe a significant yield of η signals with statistical significance more than 5σ for data at $\sqrt{s} = 4.190$, 4.210, 4.220, 4.245, 4.360 and 4.420 GeV. The number of events and the statistical significance of the η signal for these samples are listed in Table I. The scatter plots of the invariant mass of the lepton pairs $[M(\ell^+\ell^-)]$ versus that of the two photons $[M(\gamma\gamma)]$ and fit results of the η signal for data taken at $\sqrt{s} = 4.360$ GeV are illustrated in Figs. 1(e) and 1(f) and Figs. 2(e) and 2(f), respectively. For the other nine data samples at $\sqrt{s} = 3.810$, 3.900, 4.090, 4.310, 4.390, 4.470, 4.530, 4.575 and 4.600 GeV, the statistical significances of the η signal are found to be less than 5σ, and the upper limits at the 90% confidence level (C.L.) on the Born cross section are determined. Due to the large background from Bhabha events in the $J/\psi \to e^+e^-$ decay mode, only the decay mode $J/\psi \to \mu^+\mu^-$ is considered when setting the upper limit. Since the statistics are low, the number counting method is performed to extract the number of signal and background events to avoid the large uncertainty of background shape. The number of observed signal events is obtained by counting the entries in the η signal region $[0.518 < M(\gamma\gamma) < 0.578\ \mathrm{GeV}/c^2]$. The number of background events in the signal region is estimated with the events in the η sideband region or J/ψ sideband region (with an additional η signal mass window requirement) corrected with a factor. The correction factors, which take into account the difference of the number of background events in the signal region and sideband regions, are extracted by fitting on the $M(\gamma\gamma)$ distributions for the data samples with high statistics. The η sideband region is defined as $0.383 < M(\gamma\gamma) < 0.503\ \mathrm{GeV}/c^2$ and $0.593 < M(\gamma\gamma) < 0.713\ \mathrm{GeV}/c^2$, where their sizes are four times as that of the signal region. The results are all listed in Table II.

The Born cross section is calculated by

$$\sigma^B = \frac{N^{\rm obs}}{\mathcal{L}_{\rm int}\cdot(1+\delta^r)\cdot(1+\delta^v)\cdot\epsilon\cdot\mathcal{B}}, \quad (1)$$

where $N^{\rm obs}$ is the number of observed signal events, $\mathcal{L}_{\rm int}$ is the integrated luminosity, $(1+\delta^r)$ is the ISR correction factor which is obtained by QED calculation [33] and taking the line shape of the Born cross section measured by the Belle experiment [18]. The vacuum polarization factor $(1+\delta^v)$ is taken from a QED calculation with an accuracy of 0.5% [34], ϵ is the detection efficiency including reconstruction and all selection criteria, $\mathcal{B}$ is the product branching ratio and $\mathcal{B}(J/\psi\to\ell^+\ell^-)\cdot\mathcal{B}(\eta\to\gamma\gamma)$, taken from the Particle Data Group (PDG) [35].

The final Born cross sections of $e^+e^-\to\eta J/\psi$ at energy points with a statistically significant observation of signal events are listed in Table I.

For the other energy points where the η signal is not significant, we set upper limits at the 90% C.L. on the Born cross section. The upper limit is calculated by a frequentist method with a profile likelihood treatment of systematic uncertainties taken into account in the efficiency uncertainty, which is implemented by a C++ class TROLKE in the ROOT framework [36]. The numbers of observed signal events and estimated background events are assumed to follow a Poisson distribution, and the efficiencies are assumed to have Gaussian uncertainties. Since the number of background events can be estimated from either the η or J/ψ sideband events, the one with the larger upper limit on the Born cross section is taken as the final result as a conservative estimation. The results on the upper limits are listed in Table II. Another approach using the Bayesian method by fitting the $M(\gamma\gamma)$ distribution is implemented to extract the upper limit on the Born cross section, a consistent result is achieved.

Since there is no significant signal of $e^+e^-\to\pi^0J/\psi$ observed at any energy, we set upper limits at the 90% C.L. on the Born cross section. The number of observed events is obtained by counting the entries in the π^0 signal region $[0.120 < M(\gamma\gamma) < 0.150\ {\rm GeV}/c^2]$. The number of background events in the signal region is estimated by counting the number of events in the π^0 sideband regions $[0.055 < M(\gamma\gamma) < 0.115\ {\rm GeV}/c^2$ and $0.155 < M(\gamma\gamma) < 0.215\ {\rm GeV}/c^2]$ or the J/ψ sideband regions (with an additional π^0 signal mass window requirement). The same frequentist method is implemented to extract the upper limits. The results and the related variables used to calculate the upper limit are listed in Table III.

TABLE III. Upper limits of $e^+e^-\to\pi^0J/\psi$. The table shows the number of observed events in the π^0 signal region $N^{\rm sg}$, number of events in the π^0 sideband $N^{\rm sb}_{\pi^0}$ and in the J/ψ sideband $N^{\rm sb}_{J/\psi}$, efficiency ϵ, the upper limit of signal events with the consideration of the selection efficiency $N^{\rm up}(\mu^+\mu^-)/\epsilon$ (at the 90% C.L.) and the upper limit of Born cross sections $\sigma^B_{\rm up}$ (at the 90% C.L.).

$\sqrt{s}$ (GeV)	$N^{\rm sg}$	$N^{\rm sb}_{\pi^0}$	$N^{\rm sb}_{J/\psi}$	ϵ(%)	$N^{\rm up}/\epsilon$	$(1+\delta^r)$	$(1+\delta^v)$	$\sigma^B_{\rm up}$ (pb)
3.810	1	4	1	16.9	<20.2	1.243	1.056	<5.2
3.900	0	1	2	29.2	<6.0	0.775	1.049	<2.4
4.090	0	0	2	25.7	<7.8	1.078	1.052	<2.2
4.190	0	0	0	29.9	<6.7	0.866	1.056	<2.9
4.210	1	1	1	29.0	<11.8	0.914	1.057	<3.8
4.220	0	1	0	28.5	<7.0	0.937	1.057	<2.2
4.230	4	16	13	28.1	<18.5	0.960	1.056	<0.3
4.245	1	1	2	27.3	<12.6	0.992	1.056	<3.7
4.260	3	8	10	26.5	<18.8	1.021	1.054	<0.4
4.310	0	0	0	24.6	<8.3	1.105	1.053	<2.7
4.360	2	3	4	23.5	<19.9	1.168	1.051	<0.5
4.390	1	0	1	23.1	<16.0	1.198	1.051	<3.9
4.420	2	7	20	22.7	<16.3	1.225	1.053	<0.2
4.470	0	0	4	22.3	<8.9	1.258	1.055	<1.0
4.530	0	1	2	21.8	<8.9	1.295	1.055	<0.9
4.575	0	0	2	21.7	<9.2	1.314	1.055	<2.4
4.600	3	5	7	21.6	<26.2	1.323	1.055	<0.6

V. SYSTEMATIC UNCERTAINTIES

Several sources of systematic uncertainties are considered in the measurement of the Born cross sections. These include differences between the data and the MC simulation for the tracking efficiency, photon detection, kinematic fit, mass window requirement, the fit procedure, the shower depth in the MUC, the MC simulation of the ISR correction factor and the vacuum polarization factor, as well as uncertainties in the branching fractions of intermediate state decays and in the luminosity measurements.

(a) *Tracking*.—The uncertainty of the tracking efficiency is investigated using a control sample $\psi(3686)\to\pi^+\pi^-J/\psi$ with the subsequent decay of $J/\psi\to\ell^+\ell^-$. The difference in tracking efficiency for the lepton reconstruction between the data and the MC simulation is estimated to be 1% per track. So, 2% is taken as the systematic uncertainty for the two leptons.

(b) *Photon detection efficiency*.—The uncertainty due to the photon detection and reconstruction efficiency is 1% per photon [37]. This value is determined from studies using background-free control samples $J/\psi\to\rho^0\pi^0$ and $e^+e^-\to\gamma\gamma$. Therefore, an uncertainty of 2% is taken for the detection efficiency of two photons.

(c) *Kinematic fit*.—In order to reduce the difference on the $4C$ kinematic fit χ^2_{4C} between data and MC simulations, the track helix parameters (ϕ_0, κ, $\tan\lambda$) of simulated tracks have been corrected, where ϕ_0 is the azimuthal angle that specifies the pivot with respect to the helix center, κ is the reciprocal of the transverse momentum and $\tan\lambda$ is the slope of the track. The correction factors are obtained from a nearly background-free sample of $e^+e^-\to\pi^+\pi^-J/\psi$

and $J/\psi \to e^+e^-/\mu^+\mu^-$ at $\sqrt{s} = 4.230$ GeV. An alternative detector efficiency is evaluated with the same MC samples, but without helix parameter corrections. The difference in this efficiency from its nominal value is taken to be the uncertainty due to the 4*C* kinematic fit requirement [38].

(d) *Mass window requirements*.—A mass window requirement on the $\ell^+\ell^-$ invariant mass introduces a systematic uncertainty on its efficiency. The J/ψ signal at $\sqrt{s} = 4.230$ GeV is fitted with a MC shape convoluted with a Gaussian function, where the parameters of the Gaussian function are left free in the fit. To evaluate the systematic effects on the mass window requirement, the invariant mass of $\ell^+\ell^-$ in MC samples is smeared with a Gaussian function, where the parameters of the Gaussian function are obtained from the fit. The difference in the efficiencies between the signal MC sample with and without mass resolution smearing is 0.2% in the $\mu^+\mu^-$ mode and 0.1% in the e^+e^- mode, and is taken as the systematic uncertainty.

(e) *Fitting procedure*.—For the eight data samples with clearly observed η signals, fits to the two photon invariant mass $M(\gamma\gamma)$'s are performed to extract the number of $e^+e^- \to \eta J/\psi$ decays. The following three aspects are considered when evaluating the systematic uncertainty associated with the fit procedure. (1) *Fitting range*.—In the fit, the $M(\gamma\gamma)$ is fitted in a region from 0.2 to 0.9 GeV/c^2. An alternative fit with a different fit range, from 0.25 to 0.85 GeV/c^2, is performed. The differences in the yield are treated as the systematic uncertainty from the fit range. (2) *Signal shape*.—In the fit, the signal shape is described by a shape obtained from a MC simulation convoluted with a Gaussian function. An alternative fit with a Crystal Ball function [39] for the η signal shape is performed, where the parameters of the Crystal Ball function at different c.m. energies are fixed to those obtained from the fit of the η signal at $\sqrt{s} = 4.230$ GeV. The difference in the yield with respect to the nominal fit is considered to be the systematic uncertainty from the signal shape. (3) *Background shape*.—In the fit, background shapes are described as a second-order polynomial function. The fit with a third-order polynomial function for the background shape is used to estimate its uncertainty. For the data sets where no evident η signal is found, the frequentist method is employed to determine the upper limits on the Born cross section, and the numbers of signal and background events are obtained by counting the entries in the signal and sideband regions. Two different sideband regions, the η sideband region and the J/ψ sideband region, are used to estimate the uncertainty from the background shape. The systematic uncertainty associated with the background shape has been considered by taking the most conservative upper limit as the final result.

(f) *MUC requirement*.—In the search for the process $e^+e^- \to \pi^0 J/\psi$, an additional requirement on the hit depth in the MUC for muon tracks was imposed to remove the background from $e^+e^- \to \pi^+\pi^-\pi^0$. When studying the control sample of $e^+e^- \to \pi^+\pi^- J/\psi$ with a subsequent decay of $J/\psi \to \mu^+\mu^-$ at $\sqrt{s} = 4.230$ GeV, the efficiency difference of this requirement between the data and the MC sample was found to be $(9.0 \pm 1.2)\%$. The MC efficiency has been corrected for this difference and a value of 1.2% is taken as the corresponding systematic uncertainty.

(g) *ISR factor*.—The uncertainties of the line shape of the cross section used in the KKMC generator introduce uncertainties in both the radiative correction factor and the efficiency. In the nominal results, the line shape of

TABLE IV. Summary of systematic uncertainties (%) in the cross section of $e^+e^- \to \eta J/\psi$ for energies with significant signal in the $\mu^+\mu^-(e^+e^-)$ mode. The common uncertainties (luminosity, tracking, photon, branching fraction and others) between the two modes are shown together.

Source/$\sqrt{s}$ (GeV)	4.190	4.210	4.220	4.230	4.245	4.260	4.360	4.420
Luminosity	1.0	1.0	1.0	1.0	1.0	1.0	1.0	1.0
Tracking	2.0	2.0	2.0	2.0	2.0	2.0	2.0	2.0
Photon	2.0	2.0	2.0	2.0	2.0	2.0	2.0	2.0
Kinematic fit	0.4 (0.4)	0.4 (0.4)	0.4 (0.3)	0.4 (0.3)	0.5 (0.5)	0.4 (0.4)	0.3 (0.4)	0.4 (0.4)
Mass window	0.2 (0.1)	0.2 (0.1)	0.2 (0.1)	0.2 (0.1)	0.2 (0.1)	0.2 (0.1)	0.2 (0.1)	0.2 (0.1)
Fitting range	0.0 (1.0)	0.4 (0.7)	0.3 (2.6)	0.1 (2.2)	0.0 (1.0)	0.0 (0.6)	8.6 (7.5)	0.7 (2.1)
Signal shape	0.3 (1.1)	0.3 (1.1)	0.3 (1.1)	0.3 (1.1)	0.3 (1.1)	0.3 (1.1)	0.3 (1.1)	0.3 (1.1)
Background shape	4.6 (0.1)	3.9 (6.8)	2.8 (0.0)	0.0 (0.1)	9.7 (9.3)	0.2 (0.0)	0.5 (0.4)	0.1 (0.2)
ISR factor	0.6 (0.3)	4.3 (4.2)	4.7 (6.0)	4.2 (5.9)	4.0 (3.6)	6.6 (5.8)	9.4 (9.1)	10.5 (7.7)
Branching fraction	0.8	0.8	0.8	0.8	0.8	0.8	0.8	0.8
Others	1.0	1.0	1.0	1.0	1.0	1.0	1.0	1.0
Sum	5.7 (3.6)	6.7 (8.7)	6.4 (7.4)	5.3 (7.2)	11.0 (10.6)	7.4 (6.8)	13.2 (12.3)	11.0 (8.7)

TABLE V. Summary of systematic uncertainties (%) in the upper limit on the cross section of $e^+e^- \to \eta J/\psi$ in the $\mu^+\mu^-$ mode.

Source/$\sqrt{s}$ (GeV)	3.810	3.900	4.090	4.310	4.390	4.470	4.530	4.575	4.600
Luminosity	1.0	1.0	1.0	1.0	1.0	1.0	1.0	1.0	1.0
Tracking	2.0	2.0	2.0	2.0	2.0	2.0	2.0	2.0	2.0
Photon	2.0	2.0	2.0	2.0	2.0	2.0	2.0	2.0	2.0
Kinematic fit	0.4	0.4	0.4	0.4	0.4	0.4	0.4	0.4	0.4
Mass window	0.2	0.2	0.2	0.2	0.2	0.2	0.2	0.2	0.2
ISR factor	0.2	1.3	6.3	0.4	9.0	2.8	1.0	1.2	0.8
Branching fraction	0.8	0.8	0.8	0.8	0.8	0.8	0.8	0.8	0.8
Others	1.0	1.0	1.0	1.0	1.0	1.0	1.0	1.0	1.0
Sum	3.3	3.5	7.1	3.3	9.6	4.3	3.4	3.5	3.4

the cross section is taken from the fit result from the Belle experiment [18]. We have also performed a new fit with three incoherent Breit-Wigner functions, including the $Y(4360)$ and a second-order polynomial function, to the same observed cross section $\sigma(e^+e^- \to \eta J/\psi)$, where the parameters of the Breit-Wigner functions are left free in the fit. With this line shape of the cross section, the variations in $(1+\delta^r)\times\epsilon$ are taken as the uncertainties.

(h) *Luminosity.*—The integrated luminosity of data samples used in this analysis are measured using large angle Bhabha events, and the corresponding uncertainties are estimated to be 1.0% [40].

(i) *Branching fractions.*—The experimental uncertainties in the branching fractions for the processes $J/\psi \to \ell^+\ell^-$, $\eta \to \gamma\gamma$ and $\pi^0 \to \gamma\gamma$ are taken from the PDG [35].

(j) *Other systematic uncertainties.*—Other sources of systematic uncertainties include the trigger efficiency, event start time determination and final-state-radiation simulation. The total systematic uncertainty due to these sources is estimated to be less than 1.0%. To be conservative, we take 1.0% as the systematic uncertainty.

Assuming all of the above systematic uncertainties, shown in Tables IV, V and VI, are independent, the total systematic uncertainties are obtained by adding the individual uncertainties in quadrature.

For the energy points where statistically significant signal yields were found, the results from the two J/ψ decay modes are found to be consistent. The combined cross sections are calculated by considering the correlation of uncertainties between these two measurements [41] and the results are also listed in Table I.

VI. SUMMARY AND DISCUSSION

In summary, using data samples collected with the BESIII detector at 17 energies from 3.810 to 4.600 GeV, we performed an analysis of $e^+e^- \to \eta J/\psi$. Statistically significant η signals are observed at $\sqrt{s} = 4.190$, 4210, 4220, 4230, 4245, 4260, 4360 and 4420 GeV, and the corresponding Born cross sections are measured. In addition, we searched for the process $e^+e^- \to \pi^0 J/\psi$. No significant signals are observed and the upper limits at the 90% C.L. on the Born cross section are set.

A comparison of the Born cross sections $\sigma(e^+e^- \to \eta J/\psi)$ in this measurement to that of previous results [18,26] is shown in Fig. 4, and a very good agreement is achieved. The measured Born cross sections are also compared to that of $e^+e^- \to \pi^+\pi^- J/\psi$ obtained from Belle [4]. Different line shapes are observed in these two processes, which indicates that the production mechanism of the $\eta J/\psi$ clearly differs from that of $\pi^+\pi^- J/\psi$ in the vicinity of $\sqrt{s} = 4.1$–4.6 GeV. This could indicate the existence of a rich spectrum of Y states in this energy region

TABLE VI. Summary of systematic uncertainties (%) in the cross section of $e^+e^- \to \pi^0 J/\psi$.

Source/$\sqrt{s}$ (GeV)	3.810	3.900	4.090	4.190	4.210	4.220	4.230	4.245	4.260	4.310	4.360	4.390	4.420	4.470	4.530	4.575	4.600
Luminosity	1.0	1.0	1.0	1.0	1.0	1.0	1.0	1.0	1.0	1.0	1.0	1.0	1.0	1.0	1.0	1.0	1.0
Tracking	2.0	2.0	2.0	2.0	2.0	2.0	2.0	2.0	2.0	2.0	2.0	2.0	2.0	2.0	2.0	2.0	2.0
Photon	2.0	2.0	2.0	2.0	2.0	2.0	2.0	2.0	2.0	2.0	2.0	2.0	2.0	2.0	2.0	2.0	2.0
Kinematic fit	0.4	0.4	0.4	0.4	0.4	0.4	0.4	0.4	0.4	0.4	0.4	0.4	0.4	0.4	0.4	0.4	0.4
Mass window	0.2	0.2	0.2	0.2	0.2	0.2	0.2	0.2	0.2	0.2	0.2	0.2	0.2	0.2	0.2	0.2	0.2
MUC cut	1.2	1.2	1.2	1.2	1.2	1.2	1.2	1.2	1.2	1.2	1.2	1.2	1.2	1.2	1.2	1.2	1.2
ISR factor	0.2	1.1	6.5	0.3	4.6	5.7	3.9	4.1	6.7	0.8	9.6	8.7	7.9	1.0	0.7	0.5	0.7
Branching fraction	0.6	0.6	0.6	0.6	0.6	0.6	0.6	0.6	0.6	0.6	0.6	0.6	0.6	0.6	0.6	0.6	0.6
Others	0.6	0.6	0.6	0.6	0.6	0.6	0.6	0.6	0.6	0.6	0.6	0.6	0.6	0.6	0.6	0.6	0.6
Sum	3.5	3.6	7.4	3.5	5.8	6.7	5.2	5.4	7.5	3.6	10.2	9.4	8.6	3.6	3.5	3.5	3.5

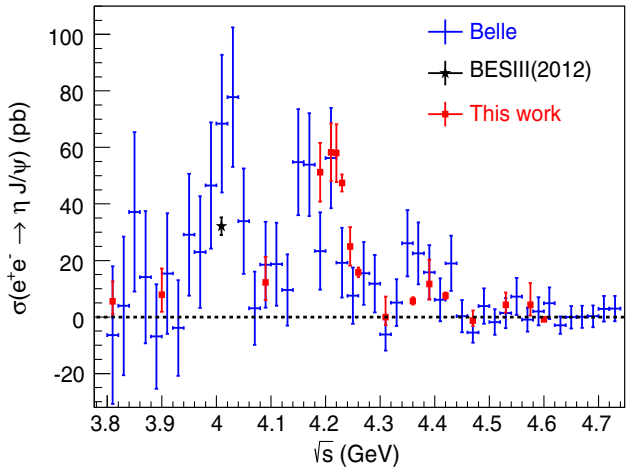

FIG. 4 (color online). A comparison of the measured Born cross section of $e^+e^- \to \eta J/\psi$ to that of previous measurements [18,26]. The blue dots are results from Belle, the black star dot is from BESIII (2012) and the red square dots are the results obtained in this work. The errors of the Belle data only include the statistical uncertainty. For the previously published BESIII results and our data, the errors reflect both statistical and systematical uncertainties.

with different coupling strengths to the various decay modes.

Compared with a theoretical prediction [25] that considers open-charm effects on the exclusive cross section line shapes of $e^+e^- \to \eta J/\psi$ and $\pi^0 J/\psi$, our results on $\eta J/\psi$ are within the range of the theoretical prediction, and the obtained $\pi^0 J/\psi$ upper limits are higher by a factor of 50 than that of the theoretical prediction.

ACKNOWLEDGMENTS

The BESIII Collaboration thanks the staff of BEPCII and the IHEP computing center for their strong support. This work is supported in part by National Key Basic Research Program of China under Contract No. 2015CB856700; the National Natural Science Foundation of China (NSFC) under Contracts No. 10935007, No. 11121092, No. 11125525, No. 11235011, No. 11322544, No. 11335008, No. 11375170, No. 11275189, No. 11079030, No. 11475164, No. 11005109, No. 11475169; the Chinese Academy of Sciences (CAS) Large-Scale Scientific Facility Program; Joint Large-Scale Scientific Facility Funds of the NSFC and CAS under Contracts No. 11179007, No. U1232201, No. U1332201; CAS under Contracts No. KJCX2-YW-N29, No. KJCX2-YW-N45; the 100 Talents Program of CAS; INPAC and the Shanghai Key Laboratory for Particle Physics and Cosmology; the German Research Foundation DFG under Contract No. Collaborative Research Center CRC-1044; the Istituto Nazionale di Fisica Nucleare, Italy; the Ministry of Development of Turkey under Contract No. DPT2006K-120470; Russian Foundation for Basic Research under Contract No. 14-07-91152; U.S. Department of Energy under Contracts No. DE-FG02-04ER41291, No. DE-FG02-05ER41374, No. DE-FG02-94ER40823, No. DESC0010118; the U.S. National Science Foundation; the University of Groningen (RuG) and the Helmholtzzentrum fuer Schwerionenforschung GmbH (GSI), Darmstadt; the WCU Program of the National Research Foundation of Korea under Contract No. R32-2008-000-10155-0.

[1] B. Aubert *et al.* (*BABAR* Collaboration), Phys. Rev. Lett. **95**, 142001 (2005); J. P. Lees *et al.* (*BABAR* Collaboration), Phys. Rev. D **86**, 051102(R) (2012).
[2] B. Aubert *et al.* (*BABAR* Collaboration), Phys. Rev. Lett. **98**, 212001 (2007); J. P. Lees *et al.* (*BABAR* Collaboration), Phys. Rev. D **89**, 111103(R) (2014).
[3] C. Z. Yuan *et al.* (Belle Collaboration), Phys. Rev. Lett. **99**, 182004 (2007).
[4] Z. Q. Liu *et al.* (Belle Collaboration), Phys. Rev. Lett. **110**, 252002 (2013).
[5] X. L. Wang *et al.* (Belle Collaboration), Phys. Rev. Lett. **99**, 142002 (2007).
[6] X. L. Wang *et al.* (Belle Collaboration), arXiv:1410.7641.
[7] Q. He *et al.* (CLEO Collaboration), Phys. Rev. D **74**, 091104(R) (2006).
[8] T. Barnes, S. Godfrey, and E. S. Swanson, Phys. Rev. D **72**, 054026 (2005).
[9] B. Aubert *et al.* (*BABAR* Collaboration), Phys. Rev. D **76**, 111105(R) (2007); **79**, 092001 (2009); G. Pakhlova *et al.* (Belle Collaboration), Phys. Rev. Lett. **98**, 092001 (2007); Phys. Rev. D **77**, 011103(R) (2008); Phys. Rev. Lett. **100**, 062001 (2008); Phys. Rev. D **80**, 091101(R) (2009).
[10] T. E. Coan *et al.* (CLEO Collaboration), Phys. Rev. Lett. **96**, 162003 (2006).
[11] J. Z. Bai *et al.* (BES Collaboration), Phys. Rev. Lett. **88**, 101802 (2002).
[12] M. Ablikim *et al.* (BESIII Collaboration), Phys. Rev. Lett. **110**, 252001 (2013).
[13] T. Xiao, S. Dobbs, A. Tomaradze, and K. K. Seth, Phys. Lett. B **727**, 366 (2013).
[14] M. Ablikim *et al.* (BESIII Collaboration), Phys. Rev. Lett. **112**, 022001 (2014).
[15] M. Ablikim *et al.* (BESIII Collaboration), Phys. Rev. Lett. **111**, 242001 (2013).
[16] M. Ablikim *et al.* (BESIII Collaboration), Phys. Rev. Lett. **112**, 132001 (2014).
[17] M. Ablikim *et al.* (BESIII Collaboration), Phys. Rev. Lett. **113**, 212002 (2014).

[18] X. L. Wang *et al.* (Belle Collaboration), Phys. Rev. D **87**, 051101(R) (2013).
[19] M. Ablikim *et al.* (BESIII Collaboration), Phys. Rev. Lett. **114**, 092003 (2015).
[20] F. E. Close and P. R. Page, Phys. Lett. B **628**, 215 (2005); S. L. Zhu, Phys. Lett. B **625**, 212 (2005); E. Kou and O. Pene, Phys. Lett. B **631**, 164 (2005); X. Q. Luo and Y. Liu, Phys. Rev. D **74**, 034502 (2006).
[21] D. Ebert, R. N. Faustov, and V. O. Galkin, Phys. Lett. B **634**, 214 (2006); L. Maiani, V. Riquer, F. Piccinini, and A. D. Polosa, Phys. Rev. D **72**, 031502(R) (2005); T. W. Chiu and T. H. Hsieh (TWQCD Collaboration), Phys. Rev. D **73**, 094510 (2006).
[22] X. Liu, X. Q. Zeng, and X. Q. Li, Phys. Rev. D **72**, 054023 (R) (2005); C. F. Qiao, Phys. Lett. B **639**, 263 (2006); C. Z. Yuan, P. Wang, and X. H. Mo, Phys. Lett. B **634**, 399 (2006).
[23] Y. P. Kuang, Front. Phys. China **1**, 19 (2006).
[24] C. F. Qiao and R. L. Zhu, Phys. Rev. D **89**, 074006 (2014).
[25] Q. Wang, X. H. Liu, and Q. Zhao, Phys. Rev. D **84**, 014007 (2011).
[26] M. Ablikim *et al.* (BESIII Collaboration), Phys. Rev. D **86**, 071101(R) (2012).
[27] T. E. Coan *et al.* (CLEO Collaboration), Phys. Rev. Lett. **96**, 162003 (2006).
[28] M. Ablikim *et al.* (BESIII Collaboration), Nucl. Instrum. Methods Phys. Res., Sect. A **614**, 345 (2010).
[29] E. V. Abakumova *et al.*, Nucl. Instrum. Methods Phys. Res., Sect. A **659**, 21 (2011).
[30] S. Agostinelli *et al.* (GEANT4 Collaboration), Nucl. Instrum. Methods Phys. Res., Sect. A **506**, 250 (2003).
[31] S. Jadach, B. F. L. Ward, and Z. Was, Comput. Phys. Commun. **130**, 260 (2000); Phys. Rev. D **63**, 113009 (2001).
[32] A. Fotopoulos, and M. Tsulaia , Int. J. Mod. Phys. A **24**, S1 (2009); R. G. Ping, Chin. Phys. C **32**, 599 (2008); D. J. Lange, Nucl. Instrum. Methods Phys. Res., Sect. A **462**, 152 (2001).
[33] E. A. Kuraev and V. S. Fadin, Yad. Fiz. **41**, 733 (1985).
[34] S. Actis *et al.*, Eur. Phys. J. C **66**, 585 (2010).
[35] K. A. Olive *et al.* (Particle Data Group), Chin. Phys. C **38**, 090001 (2014).
[36] W. A. Rolke, A. M. López, and J. Conrad, Nucl. Instrum. Methods Phys. Res., Sect. A **551**, 493 (2005).
[37] M. Ablikim *et al.* (BESIII Collaboration), Phys. Rev. D **81**, 052005 (2010).
[38] M. Ablikim *et al.* (BESIII Collaboration), Phys. Rev. D **87**, 012002 (2013).
[39] T. Skwarnicki, Ph.D. thesis, Deutsches Elektronen-Synchrotron [Report No. DESY-F31-86-02, 1986]; see https://root.cern.ch/download/doc/RooFit_Users_Manual_2.91-33.pdf for the implementation used.
[40] M. Ablikim *et al.* (BESIII Collaboration), arXiv: 1503.03408.
[41] M. Ablikim *et al.* (BESIII Collaboration), Phys. Rev. D **89**, 074030 (2014).